LIMNOLOGY
and
OCEANOGRAPHY: METHODS

ASLO

Limnol. Oceanogr.: Methods 16, 2018, 390–399

doi: 10.1002/lom3.10254

Measuring the in situ tilt orientation of fish and zooplankton using stereo photogrammetric methods

Mike Levine,* **Kresimir Williams, Patrick H. Ressler**
Alaska Fisheries Science Center, National Marine Fisheries Service (NMFS), National Oceanic and Atmospheric Administration (NOAA), Seattle, Washington

Abstract

Acoustic-derived estimates of fish and zooplankton numerical and biomass density rely on knowledge of the sound scattered by an individual, known as target strength (TS). An important, but difficult to measure, factor in determining TS is the tilt orientation of animals in relation to the insonifying acoustic wave. Underwater stereo-camera systems can provide in situ tilt measurements for fish and zooplankton. We describe a protocol to remove the effects of camera pitch and roll from tilt measurements using a low-cost orientation sensor and a mathematical correction. A tank experiment indicated that tilt estimates made with corrected pitch and roll position data improved measurement accuracy as compared to those made with uncorrected position data. This experiment also provided empirical limits on the range of yaw values that allowed for accurate estimation of target tilt and length. We further tested this protocol using an in situ collection of krill stereo images collected in the Gulf of Alaska. Krill tilts calculated with pitch- and roll-corrected position data were an average of 10° different than those collected with uncorrected position data. Our pitch- and roll-correction improved the accuracy of stereo photogrammetric tilt estimation. Extending this method to appropriate spatial and temporal scales could allow for more accurate parametrization of TS models.

Acoustic-trawl surveys are commonly used to estimate fish and zooplankton numerical and biomass density over large areas. In these surveys, acoustically observed animal aggregations are sampled using trawl, net, or optical tools, and this information is used to help assign acoustic backscatter measured with an echosounder mounted on a vessel or other platform to species or group. Converting backscatter to density or biomass requires estimates of the sound scattering characteristics of the surveyed animals, known as target strength (TS; dB re 1 m^2; Simmonds and MacLennan 2005). TS broadly depends on animal morphology (including animal length and the presence or absence of a swim bladder or gas intrusion), behavior (including the tilt orientation of individuals in relation to the insonifying acoustic wave from the echosounder), and the insonifying frequency used in the survey (Horne 2003; Gauthier and Horne 2004; Simmonds and MacLennan 2005). Tilt has an especially significant effect on TS (Foote 1980; McClatchie et al. 1996; Hazen and Horne 2003) but it is difficult to measure in situ. Poorly understood in situ animal tilt distributions lead to substantial uncertainty in both zooplankton (Demer and Martin 1995; Stanton and Chu 2000; Smith et al. 2013) and fish (Foote 1980; Blaxter and Batty 1990; Hazen and Horne 2003) TS models. Acoustic surveys in which in situ TS is regularly measured, or those conducted with acoustic-optical systems that simultaneously observe species, length, and acoustic backscatter in situ (Ryan et al. 2009; Kloser et al. 2011; Kloser et al. 2013; Briseño-Avena et al. 2015) represent special cases in which estimates of tilt may not be crucial to estimating numerical and biomass density. However, TS estimates used in acoustic-trawl surveys are often provided by a model that assumes knowledge or consistency of parameters (including tilt) under survey conditions; more accurate estimation of in situ tilt can constrain variability in TS models in this common circumstance.

Underwater stereo-camera systems are regularly used to provide precise fish length measurements in both the demersal (Harvey and Shortis 1995; Williams et al. 2010; Merritt et al. 2011; Jones et al. 2012; Rooper et al. 2012) and midwater (Williams et al. 2013, Santa-Garcon et al. 2014; Williams et al. 2016a; Boldt et al. 2018) environments. While it is possible to measure the tilt orientation of fish or zooplankton using stereo photogrammetric methods, determining this tilt relative to the water surface or to an insonifying acoustic wave (unless acoustic and optical instruments are mounted in the same plane; e.g., Kloser et al. 2013) is complicated by the motion and changing orientation of stereo-camera systems during deployment. Systems are often deployed and retrieved from survey vessels via a winch cable,

*Correspondence: mike.levine@noaa.gov

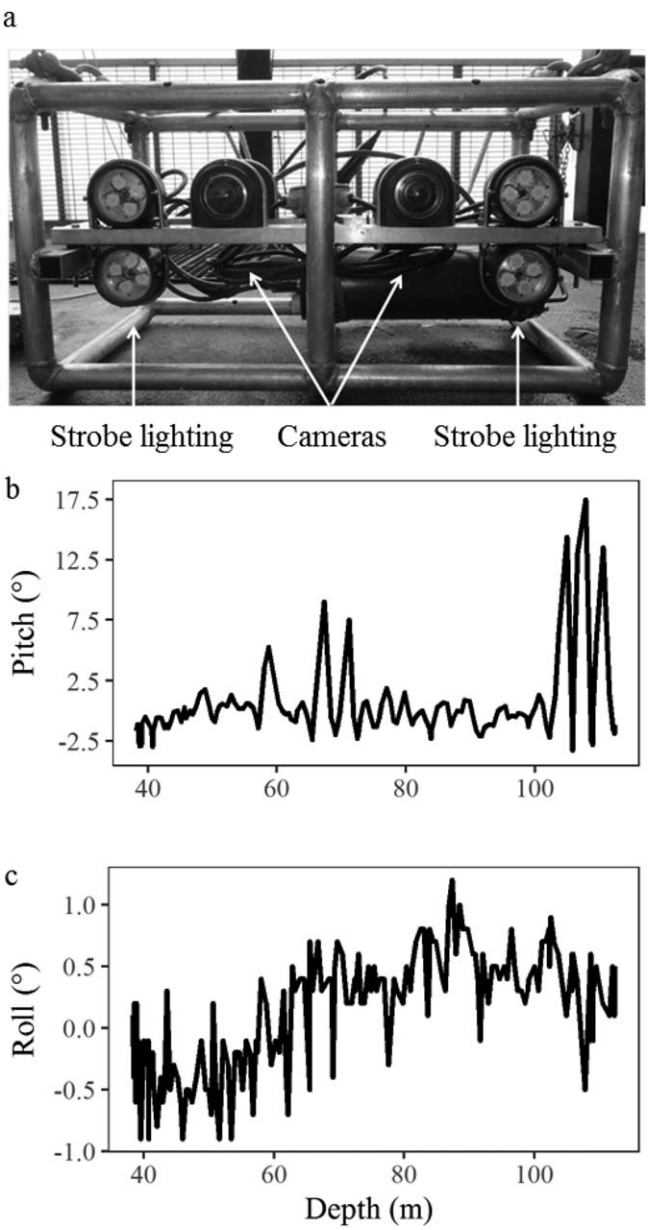

Fig. 1. (**a**) LSC. (**b**) Example of camera pitch and (**c**) example of camera roll for a single LSC deployment to the seafloor.

leading to substantial camera motion as the system is raised and lowered; animal tilt orientation measurements must be corrected for camera orientation. For example, Kubilius et al. (2015) relied on a motorized plate to maintain a horizontal camera platform and a suspended plumb line to correctly reference images to the horizontal plane in measurements of in situ euphausiid (Euphausiacea, hereafter "krill") orientation (Kubilius et al. 2015), while Boldt et al. adopted (but did not fully describe and test) the method we describe here for in situ estimates of Pacific hake (*Merluccius productus*, Boldt et al. 2018) and walleye pollock (*Gadus chalcogrammus*, Boldt et al. 2018) orientation.

We describe a protocol to effectively remove the effects of camera pitch and roll from stereo-camera-derived animal tilt orientation measurements using low-cost sensors and a mathematical rotation adjustment protocol. We further explore the effects of animal yaw in relation to the camera system on the accuracy of tilt and length measurements. Finally, we test our protocol in situ using opportunistically collected stereo images of krill obtained in the Gulf of Alaska.

Materials and procedures

Lowered stereo-camera design

The lowered stereo-camera (LSC) system used in the current study is similar in design to that described in Rooper et al. (2016). It consisted of two machine vision cameras spaced 20 cm apart, a computer to process and store images, and four white LED strobe lights (Fig. 1a). The system was powered by a 24 V battery pack and housed in a protective aluminum cage. It was connected to an electric winch at the surface via a coaxial cable. The cable also transmitted images in real-time from a single camera to the surface, allowing an operator to adjust the system relative to the sea floor in response to changes in topography. The LED strobes were triggered at a rate of 10 Hz, enabling good control of the LSCs descent as it approached the sea floor. However, only every 10^{th} pair of synchronous images was stored to the computer hard drive, resulting in an image capture rate of 1 Hz. Sensor data including camera pitch and roll were obtained from a solid-state tilt-compensated compass (OceanServer Technologies OS5000-USD model, Fall River, Massachusetts*; specified pitch and roll accuracy ± 1°, example output in Fig. 1b,c), and depth was measured using an integrated pressure sensor. These data were stored as metadata with each acquired image. The specific sensor used in this system is no longer available and we have switched to using a nine-axis absolute orientation sensor (Bosch BNO055 model, Germany) in our updated systems. This low-cost sensor also returns accurate pitch and roll data and all subsequent analyses remain identical.

Test tank experiment

We tested the effectiveness of the mathematical camera pitch and roll correction in a laboratory tank experiment. This experiment also provided a test of the accuracy of tilt and length estimates in relation to camera yaw. A test object with a horizontal base and a 45° extension was placed in a tank with the 45° extension marked at a 10.2-cm interval. The LSC was then placed ~ 1.5 m away from the test object and the test object was rotated in stages from – 90° to + 90° in relation to the LSC. These data were collected while the LSC was in a level position. Then, the LSC was then pitched

*Reference to trade names does not imply endorsement.

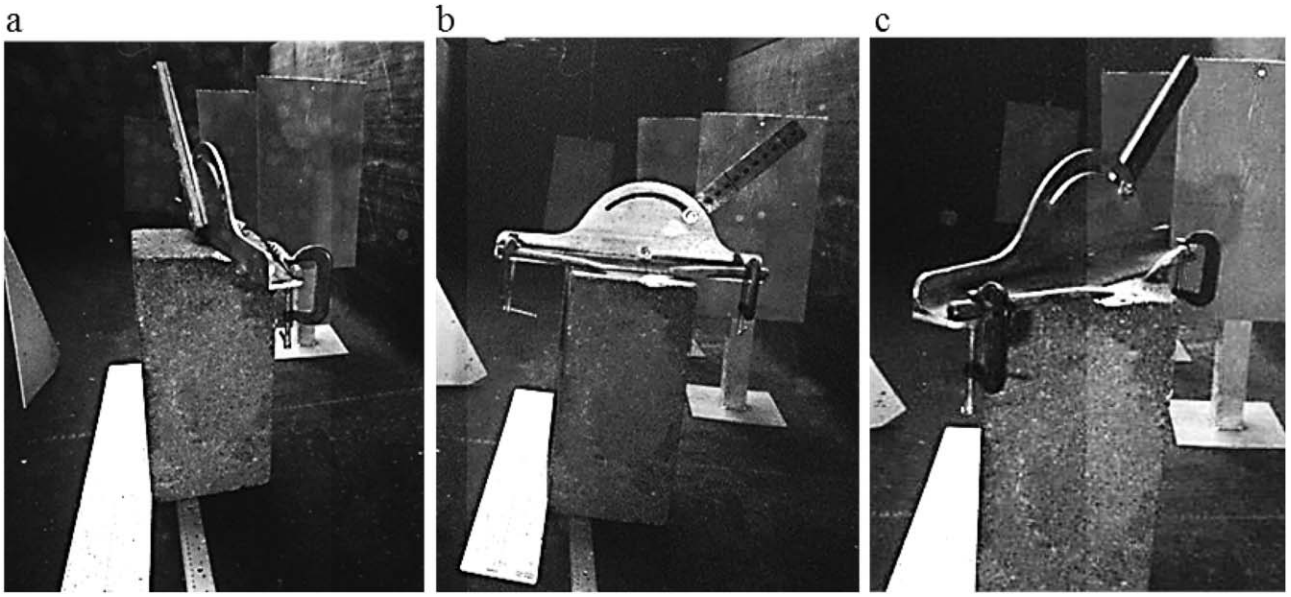

Fig. 2. Example images from the left camera of the LSC in test tank. The test object with fixed 45° angle is pictured at various camera pitch and roll angles. (**a**) Test object viewed at – 62° yaw angle, (**b**) test object viewed at 0° yaw angle, and (**c**) test object viewed at 62° yaw angle.

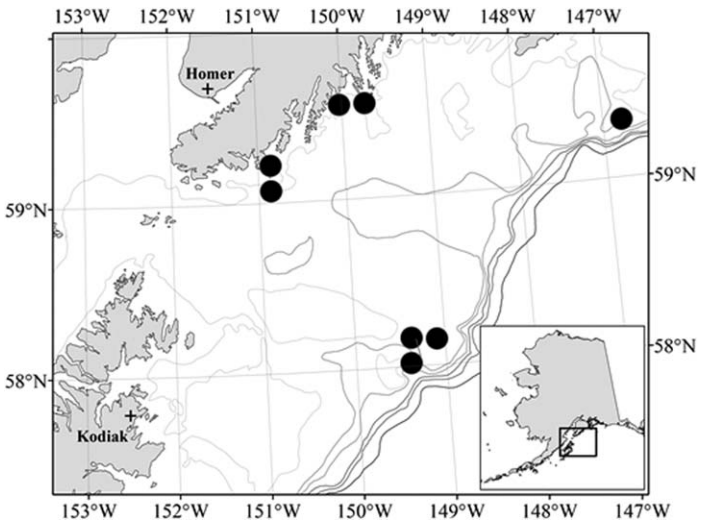

Fig. 3. Locations of eight LSC deployments (black circles) in the northern Gulf of Alaska.

downward and the test object was rotated again. Finally, this process was repeated with the LSC rolled to the left and right to capture the majority of the positions encountered during deployment (Fig. 2).

In situ image collection

We additionally collected in situ krill images during the 2015 NMFS Alaska Fisheries Science Center (AFSC) acoustic-trawl survey aboard the NOAA ship *Oscar Dyson*. As part of survey operations, the LSC was routinely deployed to assess demersal fish and habitat characteristics. While assessing krill was not a primary goal of this effort, eight LSC deployments opportunistically captured krill images while the LSC was lowered to and raised from the seafloor. These deployments were made from 29 July to 8 August 2015 offshore of the Kenai Peninsula in the northern Gulf of Alaska (Fig. 3). All deployments were performed at night (00:00 h to 06:00 h local time). Krill images were captured at depths ranging from 10 m to 170 m. Although species identification was not possible using these images, the most common krill species occurring in this area are *Thysanoessa spinifera*, *Thysanoessa inermis*, and *Euphausia pacifica*, with mean length of about 19 mm for juvenile and adult animals (Coyle and Pinchuk 2005; Simonsen et al. 2016).

LSC calibration and stereo image analysis

The LSC was calibrated in a test tank using methods introduced by Zhang (1999) and described for an underwater application in Williams et al. (2010). Briefly, the calibration routine utilized the freely available MATLAB camera calibration toolbox (Bouguet 2008) to correct for image distortion caused by the lens and camera housing viewport and to estimate the relative inter-camera geometry of the stereo-camera pair. SEBASTES, an image analysis program developed at the AFSC (Williams et al. 2016b), was then used to view and annotate synchronous image pairs. This software calculated the 3D position of the krill head and tail points identified by an analyst in both frames of an image pair by stereo triangulation using the calculated calibration parameters (Williams et al. 2010).

The 3D coordinates of individual targets identified in image pairs were then corrected for the pitch and roll of the stereo-camera system. Coordinates were adjusted to be relative to an absolute plane in which the camera optical axis

was perfectly level (0° tilt) and the optical center of both cameras was at the same height (0° roll) using a three axis rotation matrix (Arfken and Weber 2005), taking the tilt and roll values from the orientation sensor as the inputs:

$$R=\begin{bmatrix}\cos\rho & 0 & \sin\rho\\ 0 & 1 & 0\\ -\sin\rho & 0 & \cos\rho\end{bmatrix}\begin{bmatrix}1 & 0 & 0\\ 0 & \cos\theta & -\sin\theta\\ 0 & \sin\theta & \cos\theta\end{bmatrix} \quad (1)$$

where, ρ and θ are the reverse sign camera pitch and roll angles from the sensor after subtraction of readings obtained when the frame was in a level position (this accounted for the mounting position of our sensor within the LSC, which was not perfectly level) during the laboratory tank experiment. Target endpoints were then corrected by

$$\begin{bmatrix}x'\\ y'\\ z'\end{bmatrix}=R\begin{bmatrix}x\\ y\\ z\end{bmatrix} \quad (2)$$

where, x', y', and z' are the 3D target head and tail positions corrected for camera rotation, and x, y, and z are the uncorrected 3D head and tail positions in the camera coordinate system.

Corrected 3D coordinates were then used to estimate tilt (the angle of the target body in relation to water surface or the insonifying acoustic wave) and yaw (target body movement around the vertical axis) using Cartesian to spherical coordinate transforms as

$$\text{Tilt}=\text{Tan}^{-1}\left(z'_{\text{r}}\ \sqrt{x\prime_{\text{r}}^2+y\prime_{\text{r}}^2}\right) \quad (3)$$

and

$$\text{Yaw}=\text{Tan}^{-1}\left(y'_{\text{r}}\ x'_{\text{r}}\right) \quad (4)$$

where, x'_{r}, y'_{r}, and z'_{r} are the camera orientation corrected coordinates of the target head relative to the tail:

$$x'_{\text{r}}=x'\text{head}-x'\text{tail} \quad (5)$$

$$y'_{\text{r}}=y'\text{head}-y'\text{tail} \quad (6)$$

$$z'_{\text{r}}=z'\text{head}-z'\text{tail} \quad (7)$$

Target length was computed as the straight line Cartesian distance between endpoints:

$$\text{Length}=\sqrt{x\prime_{\text{r}}^2+y\prime_{\text{r}}^2+z\prime_{\text{r}}^2}. \quad (8)$$

Yaw was normalized so that all values were between – 90° ("head away" in relation to camera) and 90° ("head toward" in relation to camera). An example of 3D length, tilt, and yaw estimation is presented in Fig. 4.

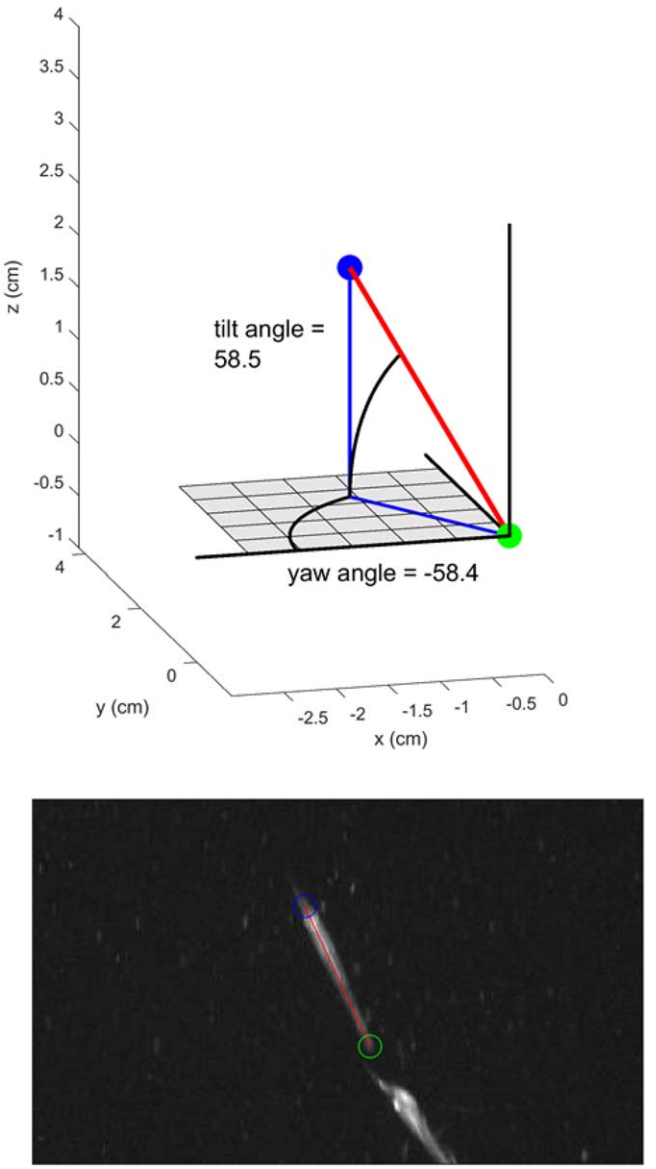

Fig. 4. Example of 3D length, tilt, and yaw estimation. Krill head and tail positions were identified and used for calculation of 3D *x*, *y*, and *z* coordinates using SEBASTES software. Tilt, yaw, and length were then calculated from these coordinates.

Selecting krill for analysis

We conservatively attempted to limit the krill used in tilt estimation to those unlikely to be disturbed by the LSC. Krill were initially categorized by body roll in relation to the sea surface and body shape. Krill roll in relation to the sea surface was categorized as dorsal side up, dorsal side down, dorsal toward camera (photophores not visible), or dorsal away from camera (photophores visible). Body shape was categorized as nearly straight, L-curved (body forms a 90° angle), or C-curved (body in "tail-flip" disturbance posture; O'Brien 1987; Lawson et al. 2006). Krill that were in focus in both camera frames and displayed a nearly straight body position

were assessed for body length, defined as the straight-line distance from the anterior of the eye to the tip of the telson. Krill that were oriented dorsal side up with a nearly straight body shape were included in the tilt analysis. Other roll and body shape characteristics were eliminated because they did not allow for a clear view of the entire krill body (dorsal away from camera and dorsal towards camera) or because the krill was displaying a potential disturbed behavioral response (defined as L- or C-shaped body positions and/or dorsal side down roll). Tilt was obtained from the length endpoints for krill used for length analysis or the endpoints of a straight line in the plane of the krill dorsum for krill assessed only for orientation.

Assessment

Accuracy of LSC-derived tilt and length estimates and pitch and roll corrections

The estimated tilt and length of the 45° test object was obtained at yaw angles from approximately – 90° to + 90° from 299 synchronous images in the tank experiment. The LSC captured images over a span of 24° of pitch (– 35.3° to – 11.1°, median = 23.6°, n =299) and 16° of roll (– 14.4 to + 1.4, median = – 6.4°, n = 299) during the experiment. This captured the observed in situ range of pitch (– 33.1° to + 19.1°, median = – 5.3°, n = 2147) and roll (– 8.6° to + 3.3°, median = – 0.5°, n = 2147) reasonably well given the limitations of our test tank. Due to shallow (1 m) water depth, we could only capture images of our test object at negative pitches (i.e., the LSC could only look downward). This is in contrast to in situ LSC deployment, where camera pitch ranged both above and below the horizontal plane. However, we did capture the magnitude of camera deviation that was experienced in the field (up to 33° from the horizontal plane). Further, the mathematical foundations for making the tilt corrections are not dependent on the sign of the tilt readings. We were unable to simulate vessel heave (upward/downward motion), surge (forward/aft motion), or sway (left–right motion) effects, in which the camera would be expected to remain level but move along other axes, in the test tank. It is possible that the accuracy of the pitch and roll estimation decreased with these specific vessel motions, but testing was beyond the scope of our study.

Pitch- and roll-corrected position data were visually examined to determine practical yaw limits for tilt and length estimation. The accuracy of tilt estimation decreased at extreme yaw angles. At yaw angles from – 90° to – 60°, the tilt of the fixed 45° test object was consistently underestimated by nearly 10°, while it was overestimated at extremely positive yaw angles of + 60° to + 90° (Fig. 5a). In contrast, yaw angles of – 60° to + 60° were accurately estimated (44.9° ± 1.8°, n = 242; Fig. 5a; values are reported as mean ± SD). Similarly, length estimates were more variable at extremely positive and negative yaw angles, though in all cases length was estimated within 10% of the actual length of the test object (Fig. 5b). Within this range, the length of the 10.2-cm test object was slightly overestimated (10.4

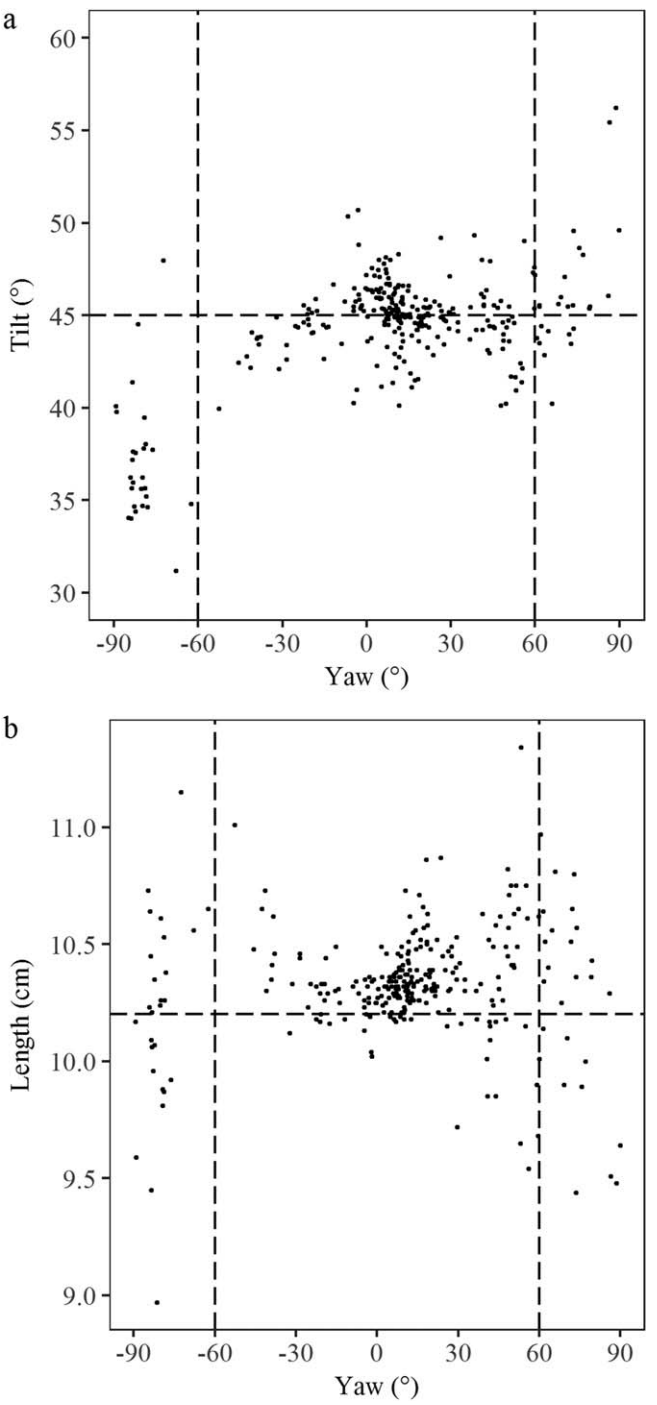

Fig. 5. (**a**) The measured tilt of a 45° test object (horizontal dashed line) at yaw angles from – 90° to + 90°. (**b**) The measured length of a 10.2 line (horizontal dashed line) at yaw angles from – 90° to + 90°. Horizontal dashed line indicates the true tilt of the test object, while vertical dashed lines indicate limits of extreme yaw angles (≤ – 60° or ≥ 60°). Targets observed at these extreme yaw angles were excluded from further analysis.

cm ± 0.2 cm, $n = 242$). Tilt and length estimates, both in the test tank and in situ, were therefore conservatively limited to objects viewed at yaw angles of – 60° to + 60°.

Poor estimates at steep yaw angles may have been due to the challenge in accurately identifying the head or tail positions of a target and/or light attenuation through the camera and housings in water (Harvey et al. 2002; Kubilius et al. 2015; Shortis 2015; Williams et al. 2016a). Our study did not attempt to determine the causes of decreased accuracy at extreme tilts. However, our results suggest that future studies using stereo photographic estimates of tilt and length should impose practical limits on the viewing angle of targets that are appropriate to the specific stereo-camera system used for the work. While limits are likely vary between specific systems due to camera placement and lens geometry, the limits we established (± 60°) are similar to limits applied in other stereo photogrammetric studies (± 25° – ± 60°; Harvey et al. 2002; Kubilius et al. 2015; Letessier et al. 2015).

The mathematical removal of camera pitch and roll improved the precision and accuracy of tilt estimates. The tilt of the 45° test object was more accurately estimated by the pitch- and roll-corrected 3D positions (44.9° ± 1.8°, $n = 242$) than by uncorrected 3D positions (41.3° ± 6.6°, $n = 242$; $t = 8.214$, df = 274.76, $p < 0.001$). Tilt estimates obtained with corrected 3D positions also displayed a relatively narrow distribution around the true 45° angle as compared to those obtained with uncorrected positions. This pattern was evident across the entire 24° span of camera pitch (Fig. 6a) and 16° span of camera roll (Fig. 6b).

In situ krill orientation and length

A total of 10,069 individual krill were identified in eight LSC deployments. Of these, 2918 krill were assessed for orientation. Eight hundred and seventy four krill were accepted for tilt estimation (i.e., dorsal side up with a nearly straight body position, yaw angle between – 60° and + 60°). On a per-krill basis, the effects of removing camera pitch and roll were substantial. The mean absolute difference between pitch- and roll-corrected tilts and uncorrected tilts was more than 10° (10.33° ± 8.19°, $n = 874$; Fig. 7a). Where the LSC platform experienced especially large pitch and roll variations from horizontal, the difference between corrected and uncorrected tilts was as great as 38.8°. In our in situ dataset, however, the differences between pre- and postcorrection tilt estimates were equally distributed around the horizontal axis and corrected values were only slightly more negative in relation to uncorrected values (– 2.97° ± 12.85°, $n = 874$; Fig. 7b).

Using the pitch- and roll-corrected 3D positions, in situ krill tilt was slightly negative (head-down) in relation to the sea surface with a wide distribution (– 8.3° ± 39.0°, $n = 874$; Fig. 8). The estimated tilt would have been ~ 3° closer to horizontal without removing the effects of camera pitch and roll.

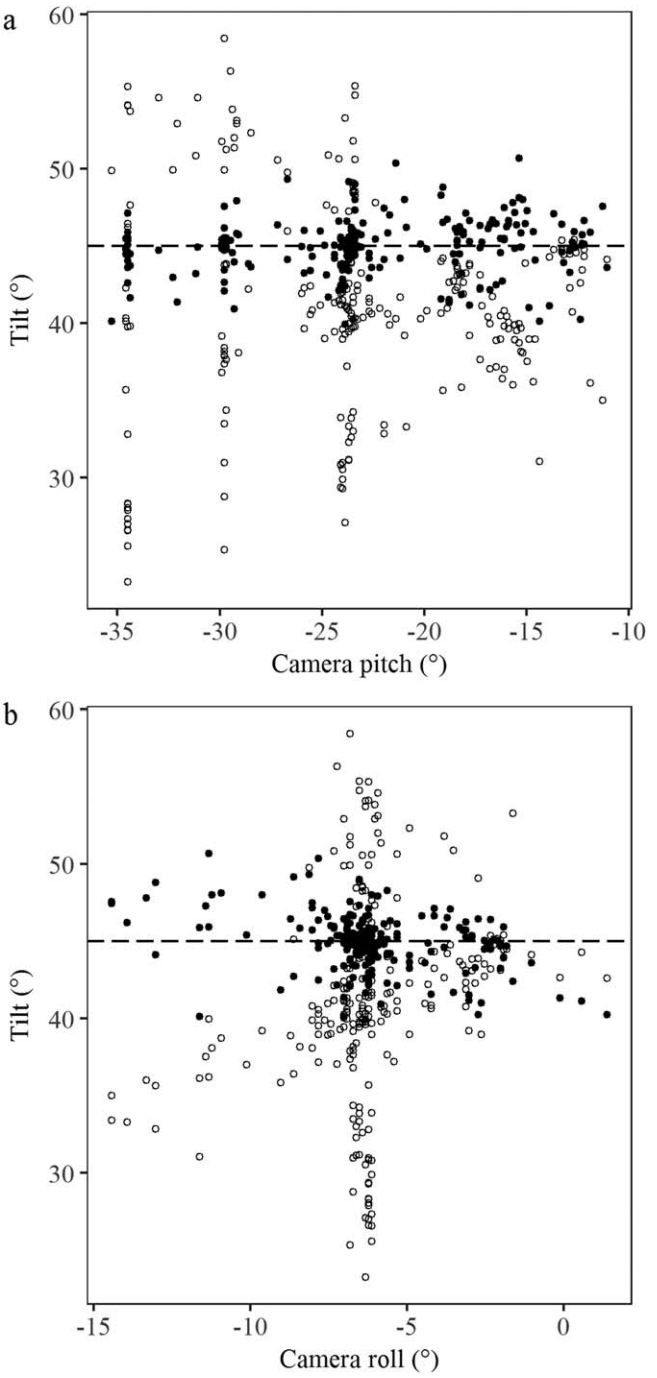

Fig. 6. LSC-estimated tilt of 45° test object using 3D coordinates both corrected for (•) and uncorrected for (○) camera (**a**) pitch and (**b**) roll. Horizontal dashed line indicates the true tilt of the test object used in test tank ($n = 242$ measurements).

Discussion

We obtained camera pitch and roll values from a commercially available pitch and roll sensor and used these values to effectively remove the effects of camera pitch and roll from stereo tilt estimates. In a test tank, estimates made

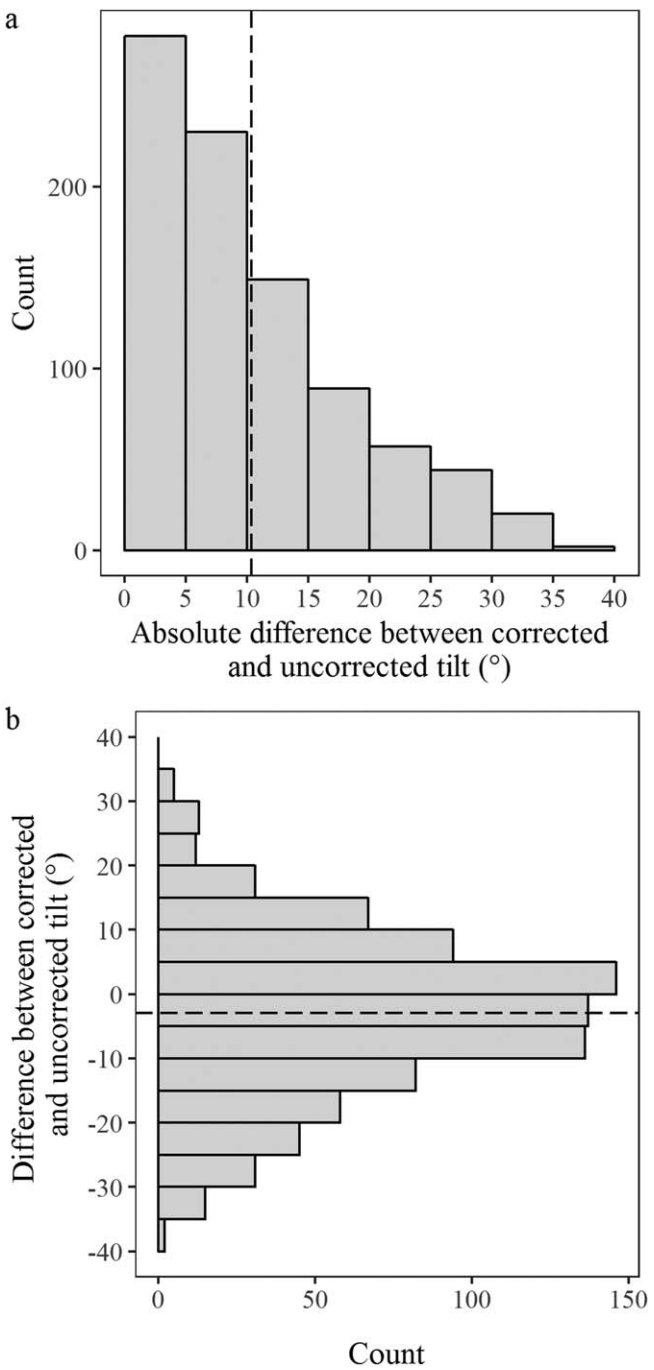

Fig. 7. (**a**) The absolute difference (°) between krill tilt estimates made using pitch- and roll-corrected position data and those made using uncorrected position data. Dashed line indicates mean absolute difference ($n = 874$). (**b**) The difference (°) between krill tilt estimates made using pitch- and roll-corrected position data and those made using uncorrected position data. Dashed line indicates mean difference, negative tilts imply head-down orientation, and positive tilts imply head-up orientation ($n = 874$).

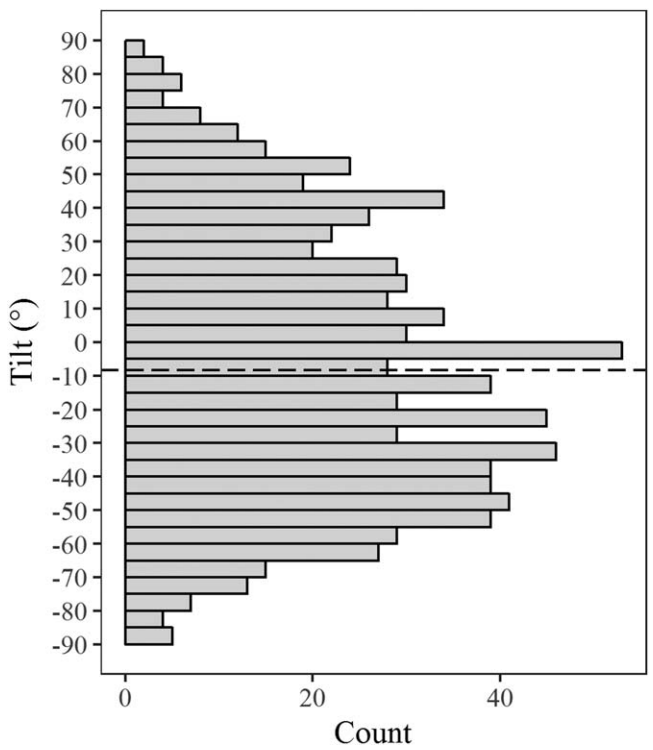

Fig. 8. Krill tilt distribution ($n = 874$). Dashed line indicates mean tilt, negative tilts imply head-down orientation, and positive tilts imply head-up orientation.

with corrected pitch and roll data accurately measured the known tilt of the test object, whereas values uncorrected for pitch and roll underestimated tilt. Applying the tilt removal protocol to our in situ collection of krill images had a strong effect on the level of individual krill: tilts calculated with pitch- and roll-corrected position data were an average of 10° different than those collected with uncorrected position data.

When our correction protocol was applied to the 874 krill assessed for tilt, mean corrected tilt was 3° more head-down than mean uncorrected tilt. Because both the distribution of krill tilts and the errors associated with using uncorrected tilt values were widely distributed with little head-up or head-down bias, the difference between mean uncorrected and corrected tilts was minimal in our in situ test. This may also be the case in other species with a mean tilt near horizontal and a wide, symmetrical distribution of orientations, such as walleye pollock (Horne 2003; Boldt et al. 2018), Antarctic krill (*Euphausia superba*; Lawson et al. 2006; Kubilius et al. 2015), and the krill species *Meganyctiphanes norvegica*, *T. inermis*, and *T. raschii* in the North Atlantic (Kristensen and Dalen 1986). However, this tilt distribution may not be representative of other commonly surveyed fish and zooplankton species. Other fish species, including Pacific hake (Boldt et al. 2018) and Norwegian herring (Huse and Ona 1996), demonstrate mean head-down or head-up orientations on average. Mean head-up or head-down orientations for species that are

typically oriented horizontally can also occur under particular circumstances, such as during diurnal behavioral changes (Huse and Ona 1996) or vessel avoidance behavior (Mitson 1995). In the case of relatively narrow tilt distributions, errors from uncorrected tilt measurement may have a larger effect on mean tilt estimates.

The krill TS model described by Smith et al. (2013) and parameterized as in Ressler et al. (2012; their table 1, Med σ_{bs} scenario) predicts a TS of – 94.4 dB for an animal 18 mm in length, assuming the distribution of krill tilt is normal with mean 0° and standard deviation 30° (Kristensen and Dalen 1986). Without new measurements, assumed krill tilt distributions based on the relatively few available literature values suggest a large range of TS is possible (e.g., 150% based on tilt scenarios in Ressler et al. 2012). Uncorrected (– 5.33° ± 37.5°, $n = 874$) and corrected (– 8.33° ± 39.5°, $n = 874$) tilt distributions we observed in the present study had a relatively wide distribution and were similar both to each other and to the Med σ_{bs} scenario in Ressler et al. (2012); thus, they led to relatively modest differences in predicted TS using the same TS model ($\sim$ 20% and 26%, respectively). However, without observations obtained using the method presented here, it would not be possible to know this, and thus better understand and constrain variability in TS due to krill orientation.

Because our camera deployments were made opportunistically, they were not structured to account for known diel patterns in krill behavior (Mauchline and Fisher 1969). In addition, the LSC described here was not deployed specifically for observing krill, and the relatively high proportion of disturbed individuals reported here could reflect a response to pressure waves created by the LSC itself as well as consistent exposure to strobing LED lighting (10 Hz). In future studies, the LSC could be lowered into an acoustic layer of interest and then allowed to sit relatively motionless while the strobes are triggered less frequently to potentially reduce disturbing stimuli. Similarly, future studies could utilize red strobe lights. The peak spectral sensitivity for many pelagic crustacean species is in the blue-green region (wavelengths $\sim$ 460–515 nm; Boden and Kampa 1965; Frank and Widder 1999), and krill are likely to be less visually sensitive to strobing at far-red wavelengths ($>$ 650 nm). The limitations of the current in situ collection highlight the need to design stereo-camera systems and sampling approaches that minimize animal attraction or avoidance responses and account for known patterns in animal behavior. The pitch- and roll-removal protocol presented in this study allows for accurate characterization of tilt from stereo images at a low cost in terms of equipment and processing time; when combined with appropriate sampling designs and equipment, in situ stereo imagery will be a valuable tool in accurate parametrization of fish and zooplankton TS models.

References

Arfken, G. B., and H. J. Weber. 2005. Mathematical models for physicists, 6th ed. Elsevier.

Blaxter, J. H. S., and R. S. Batty. 1990. Swimbladder ''behaviour'' and target strength. Rapp. p.-v. réun. Cons. Int. Explor. Mer. **189**: 233–244.

Boden, B. P., and E. M. Kampa. 1965. An aspect of euphausiid ecology revealed by echo-sounding in a fjord. Crustaceana **29**: 155–173. doi:10.1163/156854065X00325

Boldt, J. L., K. Williams, C. N. Rooper, R. H. Towler, and S. Gauthier. 2018. Development of stereo camera methodologies to improve pelagic fish biomass estimates and inform ecosystem management in marine waters. Fish. Res. **198**: 66–77. doi:10.1016/j.fishres.2017.10.013

Bouguet, J. Y. 2008. Camera calibration toolbox for Matlab [online]. [accessed 2016 July]. Available from http://vision.caltech.edu/bouguetj/calib_doc/index.html

Briseño-Avena, C., P. L.D., Roberts, P. J. S., Franks, and J. S., Jaffe, 2015. ZOOPS-O^2: A broadband echosounder with coordinated stereo optical imaging for observing plankton in situ. Meth. Oceanogr. **12**: 36–54. doi:10.1016/j.mio.2015.07.001

Coyle, K. O., and A. I. Pinchuk. 2005. Seasonal cross-shelf distribution of major zooplankton taxa on the northern Gulf of Alaska shelf relative to water mass properties, species depth preferences and vertical migration behavior. Deep Sea Res. Part 2 Top Stud. Oceanogr. **52**: 217–245. doi:10.1016/j.dsr2.2004.09.025

Demer, D. A., and L. V. Martin. 1995. Zooplankton target strength: Volumetric or areal dependence? J. Acoust. Soc. Am. **98**: 1111–1118. doi:10.1121/1.413609

Foote, K. G. 1980. Effect of fish behaviour on echo energy: The need for measurements of orientation distributions. ICES J. Mar. Sci. **39**: 193–201. doi:10.1093/icesjms/39.2.193

Frank, T. M., and E. A. Widder. 1999. Comparative study of the spectral sensitivities of mesopelagic crustaceans. J. Comp. Physiol. **185**: 255–265. doi:10.1007/s003590050385

Gauthier, S., and J. K. Horne. 2004. Acoustic characteristics of forage fish species in the Gulf of Alaska and Bering Sea based on Kirchhoff-approximation models. Can. J. Fish. Aquat. Sci. **61**: 1839–1850. doi:10.1139/f04-117

Harvey, E., and M. Shortis. 1995. A system for stereo-video measurement of sub-tidal organisms. Mar. Technol. Soc. J. **29**: 10–22.

Harvey, E., M. Shortis, M. Stadler, and M. Cappo. 2002. A comparison of the accuracy and precision of measurements from single and stereo-video systems. Mar. Technol. Soc. J. **36**: 38–49. doi:10.4031/0025332027 87914106

Hazen, E., and J. K. Horne. 2003. A method for evaluating the effects of biological factors on fish target strength. ICES J. Mar. Sci. **60**: 555–562. doi:10.1016/S1054-3139(03)00053-5

Horne, J. 2003. The influence of ontogeny, physiology, and behaviour on the target strength of walleye pollock (*Theragra chalcogramma*). ICES J. Mar. Sci. **60**: 1063–1074. doi: 10.1016/S1054-3139(03)00114-0

Huse, I., and E. Ona. 1996. Tilt angle distribution and swimming speed of overwintering Norwegian spring spawning herring. ICES J. Mar. Sci. **53**: 863–873. doi:10.1006/jmsc.1996.9999

Jones, D., C. D. Wilson, A. D. Robertis, C. N. Rooper, T. C. Weber, and J. L. Butler. 2012. Evaluation of rockfish abundance in untrawlable habitat: Combining acoustic and complementary sampling tools. Fish. Bull. 332–343.

Kloser, R. J., T. E. Ryan, G. J. Macaulay, and M. E. Lewis. 2011. In situ measurements of target strength with optical and model verification: A case study for blue grenadier, *Macruronus novaezelandiae*. ICES J. Mar. Sci. **68**: 1986–1995. doi:10.1093/icesjms/fsr127

Kloser, R. J., G. J. Macaulay, T. E. Ryan, and M. Lewis. 2013. Identification and target strength of orange roughy (*Hoplostethus atlanticus*) measured in situ. J. Acoust. Soc. Am. **134**: 97–108. doi:10.1121/1.4807748

Kristensen, A., and J. Dalen. 1986. Acoustic estimation of size distribution and abundance of zooplankton. J. Acoust. Soc. Am. **80**: 601–611. doi:10.1121/1.394055

Kubilius, R., E. Ona, and L. Calise. 2015. Measuring in situ krill tilt orientation by stereo photogrammetry: Examples for *Euphausia superba* and *Meganyctiphanes norvegica*. ICES J. Mar. Sci. **72**: 2494–2505. doi:10.1093/icesjms/fsv077

Lawson, G. L., P. H. Wiebe, C. J. Ashjian, D. Chu, and T. K. Stanton. 2006. Improved parameterization of Antarctic krill target strength models. J. Acoust. Soc. Am. **119**: 232–242. doi:10.1121/1.2141229

Letessier, T. B., J.-B. Juhel, L. Vigliola, and J. J. Meeuwig. 2015. Low-cost small action cameras in stereo generates accurate underwater measurements of fish. J. Exp. Mar. Biol. Ecol. **466**: 120–126. doi:10.1016/j.jembe.2015.02.013

Mauchline, J., and L. R. Fisher. 1969. The biology of euphausiids. Adv. Mar. Biol. **7**: 1–454.

McClatchie, S., J. Alsop, Y. Zhen, and R. F. Coombs. 1996. Consequence of swimbladder model choice and fish orientation to target strength of three New Zealand fish species. ICES J. Mar. Sci. **53**: 847–862. doi:10.1006/jmsc.1996.0106

Merritt, D., and others. 2011. BotCam: A baited camera system for nonextractive monitoring of bottomfish species. Fish. Bull. **109**: 56–67.

Mitson, R. B. (Ed.) 1995. Underwater noise of research vessels: review and recommendations. ICES Cooperative Research Report, 209. 61 pp.

O'Brien, D. P. 1987. Description of escape responses of krill (Crustacea: Euphausiacea), with particular reference to swarming behavior and the size and proximity of the predator. J. Crust. Biol. **7**: 449–457. doi:10.2307/1548294

Ressler, P. H., A. De Robertis, J. D. Warren, J. N. Smith, and S. Kotwicki. 2012. Developing and acoustic survey of euphausiids to understand trophic interactions in the Bering Sea ecosystem. Deep Sea Res. Part 2 Top Stud. Oceanogr. **65–70**: 184–195. doi:10.1016/j.dsr2.2012.02.015

Rooper, C. N., M. H. Martin, J. L. Butler, D. T. Jones, and M. Zimmerman. 2012. Estimating species and size composition of rockfishes to verify targets in acoustic surveys of untrawlable areas. Fish. Bull. **110**: 317–331.

Rooper, C. N., M. F. Sigler, P. Goddard, P. Malecha, R. Towler, K. Williams, R. Wilborn, and M. Zimmermann. 2016. Validation and improvement of species distribution models for structure-forming invertebrates in the eastern Bering Sea with an independent survey. Mar. Ecol. Prog. Ser. **551**: 117–130. doi:10.3354/meps11703

Ryan, T. E., R. J. Kloser, and G. J. Macaulay. 2009. Measurement and visual verification of fish target strength using an acoustic-optical system attached to a trawlnet. ICES J. Mar. Sci. **66**: 1238–1244. doi:10.1093/icesjms/fsp122

Santana-Garcon, J., B. Braccini, T. J. Langlois, S. J. Newman, R. B. McAuley, and E. S. Harvey. 2014. Calibration of pelagic stereo-BRUVs and scientific longline surveys for sampling sharks. Meth. Ecol. Evol. **5**: 824–833. doi: 10.1111/2041-210X.12216

Shortis, M. 2015. Calibration techniques for accurate measurements by underwater camera systems. Sensors **15**: 30810–30827. doi:10.3390/s151229831

Simmonds, J., and D. MaClennan. 2005. Fisheries acoustics: Theory and practice, 2nd ed. Blackwell.

Simonsen, K. A., P. H. Ressler, C. N. Rooper, and S. G. Zador. 2016. Spatio-temporal distribution of euphausiids: An important component to understanding ecosystem processes in the Gulf of Alaska and eastern Bering Sea. ICES J. Mar. Sci. **73**: 2020–2036. doi:10.1093/icesjms/fsv272

Smith, J. N., P. H. Ressler, and J. D. Warren. 2013. A distorted wave Born approximation target strength model for Bering Sea euphausiids. ICES J. Mar. Sci. **70**: 204–214. doi:10.1093/icesjms/fss140

Stanton, T. K., and D. Chu. 2000. Review and recommendations for the modelling of acoustic scattering by fluid-like elongated zooplankton: Euphausiids and copepods. ICES J. Mar. Sci. **57**: 793–807. doi:10.1006/jmsc.1999.0517

Williams, K., C. N. Rooper, and R. Towler. 2010. Use of stereo camera systems for assessment of rockfish abundance in untrawlable areas and for recording pollock behavior during midwater trawls. Fish. Bull. **108**: 352–362.

Williams, K., C. D. Wilson, and J. K. Horne. 2013. Walleye pollock (*Theragra chalcogramma*) behavior in midwater trawls. Fish. Res. **143**: 109–118. doi:10.1016/j.fishres.2013.01.016

Williams, K., N. Lauffenburger, M.-C. Chuang, J.-N. Hwang, and R. Towler. 2016a. Automated measurements of fish within a trawl using stereo images from a camera-trawl device (CamTrawl). Meth. Oceanogr. **17**: 138–152. doi: 10.1016/j.mio.2016.09.008

Williams, K., R. Towler, P. Goddard, R. Wilborn, and C. Rooper. 2016b. Sebastes stereo image analysis software. AFSC Processed Rep. 2016-03, 42 p. Alaska Fish. Sci. Cent., NOAA, Natl. Mar. Fish. Serv., 7600 Sand Point Way NE, Seattle WA 98115.

Zhang, Z. 1999. Flexible camera calibration by viewing a plane from unknown orientations. In Computer Vision. The Proceedings of the Seventh IEEE International Conference on (Vol. 1, pp. 666–673).

Acknowledgments

We would like to thank the crew of the NOAA ship Oscar Dyson for operational support during SDC deployments. In addition, N. Lauffenburger was instrumental in conducting the deployments at sea. C. Rooper generously loaned the SDC used in this study. This manuscript was greatly improved by the comments of N. Lauffenburger, C. Rooper, and C. Wilson. The recommendations and general content presented in this article do not necessarily represent the views or official position of the US Department of Commerce, the National Oceanic and Atmospheric Administration, or the National Marine Fisheries Service.

Conflict of Interest

None declared.

Submitted 2 November 2017
Revised 12 March 2018
Accepted 3 May 2018

Associate editor: Malinda Sutor